ECS Transactions, 41 (1) 131-139 (2011)
10.1149/1.3635549 ©The Electrochemical Society

# A Representative Volume Element Approach for Pore-Scale Modeling of Fuel Cell Materials

E. A. Wargo[a], A. C. Hanna[a], A. Cecen[a], S. R. Kalidindi[a,b], E. C. Kumbur[a,*]

[a] Department of Mechanical Engineering and Mechanics, Drexel University, Philadelphia, Pennsylvania 19104, USA
[b] Department of Materials Science and Engineering, Drexel University, Philadelphia, Pennsylvania 19104, USA
[*] Corresponding author (kumbur@drexel.edu)

The objective of this work is to utilize the recent advances in microstructure quantification to select small volumes (referred to as representative volume elements, or "RVEs") for use in pore scale modeling, which accurately reflect the overall microstructure and transport properties of large fuel cell material datasets. The micro-porous layer (MPL) of polymer electrolyte fuel cells is chosen for demonstration. Focused ion beam scanning electron microscopy is utilized to obtain a 3-D structural dataset for the selected MPL sample. Using *n*-point statistics, RVEs are selected from the full dataset to reflect the ensemble averaged statistics of the full dataset to within acceptable tolerance. Metric comparisons between RVEs and the full dataset indicate that the selected RVEs offer a very good representation of the full dataset, albeit in a volume that is significantly smaller in spatial extent, therefore providing a computationally efficient and reliable model domain for pore-scale modeling efforts.

## Introduction

Many of the water management problems of polymer electrolyte fuel cells (PEFCs) are believed to originate from the unique and complex internal structure (henceforth simply referred to as "microstructure") of the porous materials used in PEFCs (1-4). Due to the minute length scales and heterogeneous nature of these materials (e.g., diffusion media (DM), catalyst layer), experimental investigations to characterize the microstructure of these materials can be expensive and quite difficult to conduct, if not impossible. While modeling efforts have provided valuable new insights (4-17), significant discrepancies still exist between experimental and modeling studies. These inconsistencies likely originate from the fact that the microstructure features of the fuel cell materials are not accurately accounted for in the current modeling approaches. For instance, macroscopic models rely heavily on bulk correlations which do not adequately account for the specific microscale topology in fuel cell materials, and therefore do not provide sufficient insight regarding the role of morphological features of these materials on cell performance (2,18).

Pore-scale modeling can rectify the deficiencies of macroscopic modeling, as it can be applied directly to a more realistic representation of the microstructure. However, each pore-scale modeling technique has its own limitations. For example, pore network

modeling (7-12) is fairly computationally efficient, but utilizes highly idealized geometrical descriptions of the material's pore space. The lattice-Boltzmann (LB) (13-15) and volume of fluid (VOF) (16-17) methods can be applied to more realistic pore structures, such as those obtained using 3-D imaging techniques like X-ray computed tomography or focused ion beam scanning electron microscopy (FIB-SEM). However, since the LB and VOF methods are fairly computationally intensive, these models were limited to very small sub-volumes (~ 50 to 150 pixels$^3$ selected either randomly or by some generic averaging process) of the full dataset (over ~ 500 pixels$^3$). Considering the complex structure of fuel cell DM, it is very likely that selection of "random" small volumes will not accurately reflect the overall microstructure of the DM and result in inaccurate conclusions regarding the structure-transport-performance relationship.

Here, we show that choosing small volumes "randomly" for pore-scale analysis is unlikely to yield results which are representative of the full dataset. Therefore, a more rigorous approach is necessary to identify a representative volume element (RVE) for the full material dataset. Here, an RVE is defined as a small finite region in the material structure that is "statistically representative" of the entire sample's microstructure and represents the macroscale properties of the sample with a desired accuracy (19). The objective of this work is to explore the recently developed approach of using a weighted set of optimally selected statistical volume elements (SVEs) (referred to as a "WSVE Set") to serve as a proper RVE that accurately represent the overall microstructure and transport properties of the full dataset. The micro-porous layer (MPL) (3-4) in PEFCs is chosen for initial demonstration of the approach for application to fuel cell materials.

## Method of Approach

### Dataset Acquisition and Image Processing

As a first step to study the MPL microstructure, an FEI Strata$^{TM}$ DB 235 FIB-SEM was utilized to perform nanotomography on the MPL of a SIGRACET® SGL 10 BC gas diffusion layer. The high precision beam control/ion-milling ability enables serial cross-sectional surface slicing, which is used for 3-D visual reconstruction of the tested specimen (15,20-21). Prior to milling with the $Ga^+$ ion beam, a 1.5 μm platinum layer was deposited over the target volume of interest to prevent ion damage. Serial cross-sectional micrographs of the MPL were obtained by successively milling 20 nm slices at 500 pA/30 kV, followed by capturing an SEM image (pixel resolution ~10 nm) of the milled surface. This process resulted in a captured volume of ~ 5x8x2 μm from the tested MPL sample.

The next step is to pre-process the captured images to improve the quality of the data for further analysis. The raw FIB-SEM image sets are inherently problematic due to the off-normal angle of the SEM source and the small pore sizes in the MPL which approach the limits of FIB-SEM resolution. To address these issues, we have applied a specific image pre-processing protocol developed in house which consist of four main steps: *i*) image alignment, *ii*) viewing angle correction, *iii*) creation of cubic voxels, and *iv*) gradient removal.

Following image pre-processing, the next important task is to develop and implement an appropriate segmentation protocol for the particular microstructure dataset, to enable accurate determination of whether each pixel is occupied by the solid or the pore phase (only one is allowed in each pixel). Among the tested thresholding techniques, the iterative ISODATA method (22) was observed to perform the best for the captured MPL dataset. The segmentation process yielded a porosity measurement of 0.42±0.02 for the MPL data, in good agreement with values found in literature (23). Once segmentation is completed, the stack of binary images is combined in 3-D, forming a volumetric reconstruction of the measured microstructure (full dataset shown in Fig. 2).

Representative Volumes

Once the microstructure of the material has been captured and properly segmented to obtain a 3-D dataset, the full dataset may be analyzed to select an RVE. In this study, the novel WSVE Set approach is applied which captures the details of the microstructure in a set of small volumes optimally selected from the larger, full material dataset. Each SVE in the set is chosen using special optimization algorithms and individually weighted to best capture the selected microstructure metrics (in this case 2-point statistics) of the full dataset. In this sense, the set of weighted SVEs serves as an equivalent of an RVE. The macroscale effective value for any property ("metric") of the given material is calculated by taking the weighted average of the corresponding values for the members of the WSVE Set. The number of volume elements in the WSVE Set is selected such that the measured ensemble-averaged 2-point statistics of the full dataset are matched within acceptable tolerance (19).

Microstructure analysis was performed through a detailed investigation of 2-point statistics of the measured dataset. A 2-point statistic or 2-point correlation captures the spatial correlation between two different local states (e.g., phases) that are present in the structure. More specifically, a 2-point correlation shows the probability for which the head and tail (i.e., "two points") of a vector in a specific orientation lie in particular phases (e.g., pore, solid material). When the same local state is selected for both ends of the vector (i.e., head and tail), the 2-point correlation is referred to as an auto-correlation (24). However, if different local states are selected for both ends of the vector, the 2-point correlation is called a cross-correlation. When considering a pore-pore auto-correlation for example, both the head and the tail of the vector must lie in the pore phase of the material.

The 2-point statistics are used here to capture the important statistical measures of the structure, since they contain significant information regarding the size, shape, and spacing of features (i.e., phases) within the microstructure (19,24). As an example, a 3-D two-phase microstructure volume composed of 100x100x100 voxels requires $100^3$ 2-point statistics (dimensions) to represent it. The specific importance of any one of these statistics varies based on the structural features of the material under investigation. For this particular problem, to speed up the WSVE Set selection process, this large amount of data is adequately represented in a much lower dimensional space using principal component analysis (PCA). The PCA method decomposes the data into an orthonormal basis, ranked by order of importance (25). In the high dimensional space, the direction with the greatest scatter is chosen as the principal direction. Then, all directions normal to the principal direction are examined to find the one(s) with the most scatter. Often, only a

few basis vectors are necessary to provide an adequate representation. The specific weight of each SVE member is optimally assigned during the PCA procedure so that the 2-point statistics are best matched by the WSVE Set.

Since the properties of a material are complicated functions of its underlying structure, it is expected that an RVE that captures the structure well (e.g., through the 2-point statistics) is expected to accurately represent its effective material properties (19). For the measured MPL datasets, since only two phases (solid and pore) are considered, there is only one independent 2-point correlation (19). For convenience, this independent 2-point correlation is selected as the pore-pore auto-correlation in this study.

Evaluation of Key Metrics for WSVE Set Validation

Once a WSVE Set has been selected from the full microstructure dataset, the next step is its validation through a comparison of key structure metrics for the WSVE Set and the full material dataset. Several key microstructure metrics have been identified for this purpose, which include the porosity, internal surface area, connected internal surface area, tortuosity, and structural diffusivity coefficient. Although these metrics are used primarily to validate the WSVE Sets produced in this work, many of them are also of high importance for PEFC modeling studies.

In particular, we have taken a unique approach for the estimation of two important transport related metrics: (i) tortuosity and (ii) the structural diffusivity coefficient. Tortuosity was estimated by using Dijkstra's search algorithm (26) to identify the shortest path between a designated voxel on one face of the sample volume and the opposing face. Rather than utilizing an effective diffusion coefficient-tortuosity correlation as in (15,20), our procedure calculates the tortuosity by comparing the identified shortest path lengths for every single pore voxel on one face to the shortest distance between the opposing surfaces in a 3-D dataset. In addition, a 3-D diffusion model has been developed to evaluate the structural diffusivity coefficient, based on a finite volume approximation of the steady-state Fickian diffusion model. The structural diffusivity coefficient is selected here as an example of a basic bulk transport property that is expected to be significantly influenced by the details of the microstructure. More information regarding these algorithms can be found in our study (27).

## Results and Discussion

Selection of WSVE Sets

Prior to selecting a WSVE Set, an appropriate SVE window size and number of SVE members in the WSVE Set should be determined to ensure the accuracy of results and computational efficiency. The appropriate SVE window size was determined by performing a procedure as follows:

I. 300 random volumes of window size 100x100x100 pixels (100 pixels$^3$) were selected from the full binary dataset. The window size of 100 pixels$^3$ was chosen, because it can capture a sufficient number of structural features in the MPL upon visual inspection. The 300 volumes of 100 pixels$^3$ are also sufficient to cover the

full dataset (500x800x204 pixels) over three times, providing sufficient window overlap for computing statistical averages.

II. The 2-point statistics were calculated (via pore-pore auto-correlations on the 3-D binary volume) for each of these 300 volumes and averaged to obtain an "ensemble average" of 2-point statistics for the MPL.

III. The scalar error in 2-point statistics was then calculated for each of the individual 300 volumes versus the ensemble average.

This procedure was executed for five additional window size cases (50, 75, 125, 150, 175 pixels$^3$). In each case, the "ensemble average" or target (i.e., the average of 2-point statistics) is calculated from the 300 random volumes in the full dataset for the respective window size. The average and range of scalar statistical error are plotted in Fig. 1 for all six window sizes. As shown in Fig. 1, a very minor change in error is achieved beyond a window size of 100 pixels$^3$. Thus, a window size of 100 pixels$^3$ was deemed appropriate for WSVE Set selection to accurately reflect the structural features of the full dataset.

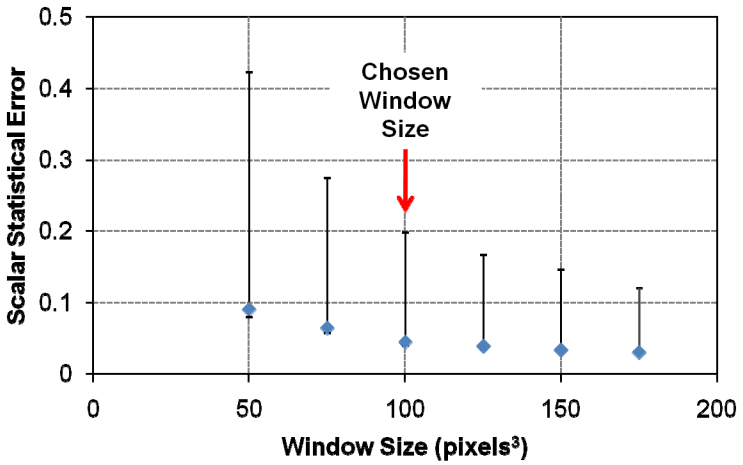


Figure 1. Plot of scalar statistical error versus window size for selection of an appropriate SVE window size, determined as 100 pixels$^3$.

Once an appropriate SVE window size is identified, the next step is to determine the number of members in a WSVE Set that is necessary to sufficiently capture the structural features of the full dataset. The appropriate number of members in the WSVE Set was determined by finding the WSVE Sets (composed of different numbers of WSVE members, optimally selected from the 300 random volumes) which most accurately reflect the 2-point statistics of the full dataset. For that purpose, WSVE Sets composed of only one member up through ten members (each member has a size of 100 pixels$^3$) were constructed and evaluated. For each of these ten WSVE Sets, the scalar statistical error in 2-point statistics between the WSVE Set and ensemble average was determined for comparison. Results showed that the drop in error beyond a 5-member WSVE Set is relatively small. Figure 2 shows the exact location of each WSVE member within the full dataset for the 1-, 3-, and 5-member WSVE Sets (analyzed below).

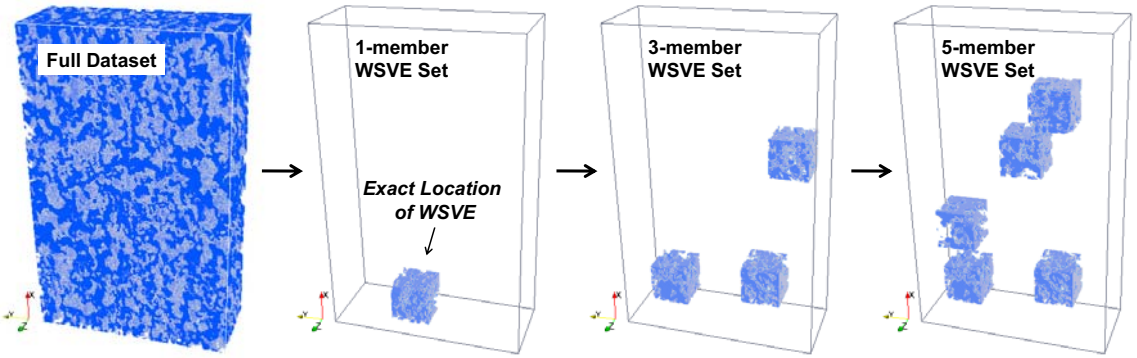


Figure 2. The exact locations of the WSVEs (each member is ~ 1x1x1 μm) within the full dataset (~ 5x8x2 μm) for the 1-, 3-, and 5-member WSVE Sets.

## WSVE Sets: Metrics and Validation

Once WSVE Sets were identified for the MPL dataset, the metric (property) analysis protocol was applied to determine the key structure and transport properties of the selected WSVE Sets, including: porosity ($\varepsilon$), internal surface area (ISA), connected internal surface area (CISA), through-plane tortuosity ($\tau$), and structural diffusivity coefficient ($K$). In order to reduce computational cost, the metrics for the full dataset were determined by averaging over the 300 random volumes to obtain an "ensemble average", whereas the WSVE Set averages were determined using the individual metric calculations for each WSVE and the corresponding weighting factor. The ensemble-averaged values and 1-, 3-, and 5-member WSVE Set averages are shown in Table I, with % errors included in red. Based on the surface area results, a 1-member WSVE Set seems insufficient, showing errors around 15%. However, all other metrics are within 5% error for all three WSVE Set sizes. The ensemble average porosity (0.41) and through-plane tortuosity (1.34) results agree well with the values reported in Ostadi *et al.* (15).

**Table I.** Structural properties of MPL obtained from WSVE Sets vs. ensemble average (full dataset).

| | Porosity | Surface Area ($\mu m^2/\mu m^3$) | Connected Surface Area ($\mu m^2/\mu m^3$) | Tortuosity | Structural Diff. Coeff. |
|---|---|---|---|---|---|
| Ensemble Average | 0.4115 | 23.77 | 22.30 | 1.34 | 0.225 |
| 1-member WSVE Set | 0.4081 | 27.52 | 25.91 | 1.35 | 0.221 |
| (% Error) | (0.84) | (15.76) | (16.19) | (0.74) | (2.13) |
| 3-member WSVE Set | 0.4110 | 24.91 | 23.35 | 1.37 | 0.222 |
| (% Error) | (0.13) | (4.76) | (4.70) | (1.88) | (1.66) |
| 5-member WSVE Set | 0.4108 | 24.23 | 22.75 | 1.36 | 0.218 |
| (% Error) | (0.18) | (1.93) | (2.04) | (1.13) | (3.28) |

As with the scalar error in 2-point statistics, the errors in metric calculations are also expected to drop as the number of members in the WSVE Set increases (see Table I). The results for surface areas (ISA and CISA) follow this trend closely, since surface area is closely related to 2-point statistics (28). Additionally, a loss in surface area of only 1.5 $\mu m^2/\mu m^3$ (6.2%) is found when ISA and CISA are compared, indicating a high pore connectivity in the MPL microstructure. Porosity is well captured by the WSVE Sets. A small increase in % error for the 5-member WSVE Set porosity value is shown in Table I, but this is likely due to the fact that all 2-point statistics (not just the 1-point statistic, equivalent to the porosity) are considered when selecting a WSVE Set. Even so, the

porosity values determined for the WSVE Sets are still in very good agreement with the ensemble average, exhibiting an error less than 1%.

Although quite acceptable, the % errors for $\tau$ and $K$ do not decrease steadily as the number of members in the WSVE Set increases (Table I). This behavior is attributed to the fact that $\tau$ and $K$ are more complex structure parameters that most likely are related to higher-order statistics (beyond the 2-point statistics). An explanation for this behavior is depicted in Fig. 3 by demonstrating two simple cases. For Case #1, the path from side A to side B in the microstructure is very short, resulting in a low $\tau$. Adding the single material pixel (highlighted in red) to the structure in Case #2 will eliminate the original path/pore region taken, drastically increasing the shortest path length from A to B (i.e., increasing $\tau$) and lowering the $K$ value significantly. However, the addition of this pixel will have minimal effect on the ensemble-averaged 2-point statistics. It should be noted that good agreement for $\tau$ and $K$ is still observed with respect to the ensemble averages, achieving consistent results well within 5% error for all three WSVE Set sizes (Table I). These results indicate that the WSVE Set approach presented in this work is indeed effective in capturing key transport related properties of a microstructure in a small volume within acceptable tolerance.

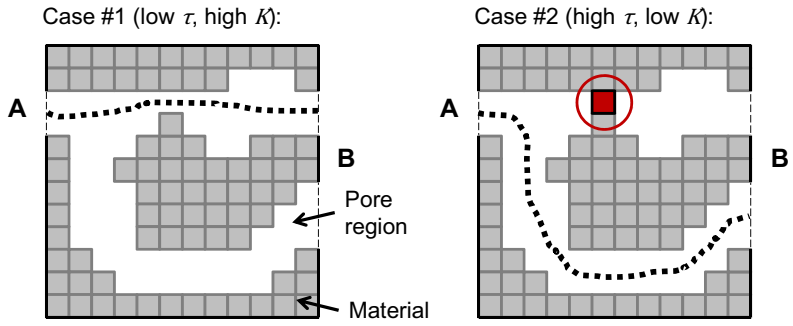


Figure 3. Adding the circled material pixel in Case #2 drastically increases the path length from side A to side B (i.e., increases $\tau$), but has minimal effect on the 2-point statistics. Adding this pixel will also lower $K$ significantly.

To further validate the WSVE Set approach, an investigation was performed in which the 5-member WSVE Set metric averages were compared with the averages obtained by selecting five random volumes. These random 5-member volume combinations were selected from the 300 random windows used for the WSVE Set selection. The five random members in each set were weighted equally when computing the metric averages, and a total of 5000 of these random volume sets were considered. Histograms composed of metric averages for the 5000 random 5-member volume sets were produced (examples shown in Fig. 4 for porosity and the structural diffusivity coefficient). For each metric histogram, a normal distribution fit is applied (shown in red), and the ensemble average and 5-member WSVE Set average are plotted as vertical lines. The ensemble average closely aligns with the peak (mean) of the normal distribution fit, indicating that 5000 random volumes are sufficient for the comparison. The results show that the majority of the 5000 random sets are less accurate than the 5-member WSVE Set (97%, 67%, 61% and 74% for $\varepsilon$, CISA, $\tau$ and $K$, respectively). More specifically, these probabilities are equal to the percentage of the 5000 random sets which have a % error (with respect to the ensemble average) that is greater than the % error of the 5-member WSVE Set for the particular metric. Therefore, these analyses indicate that a high probability exists that the

selection of a set of random volumes will be less accurate than our optimally selected WSVE Set, emphasizing the importance of the selection of proper RVE(s) for use in models.

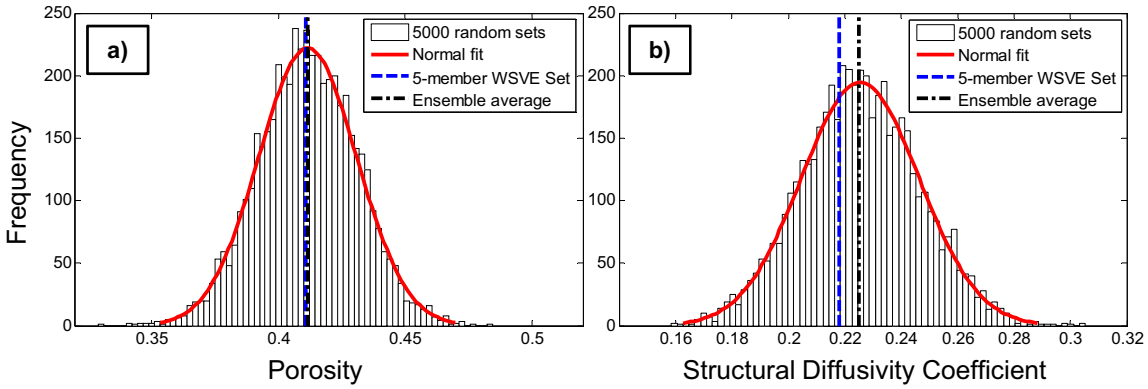


Figure 4. Histogram plots composed of metric averages for the 5000 random 5-member volume combinations, for a) porosity and b) structural diffusivity coefficient.

## Conclusions

In this work, we have presented a new approach for the selection of small RVEs, in the form of WSVE Sets, which accurately capture the properties of a large material dataset. The approach was applied to a 3-D FIB-SEM dataset for an MPL sample used in PEFCs. Computationally efficient protocols were developed and applied to the 3-D MPL dataset to determine key structure properties that are very difficult to determine by experimental means.

Small WSVE Sets composed of one, three, and five members (each ~ 1x1x1 μm in size) were selected from the full MPL dataset by matching the overall 2-point statistics. Key structure metrics were evaluated for each WSVE Set and compared with the respective values for the full MPL dataset. The comparison shows very good agreement, indicating that the WSVE Sets can indeed capture transport related properties of the full dataset with high accuracy (less than 5% error). A comparison of the metrics captured for the WSVE Sets against those captured for randomly selected volumes showed that selection of a random volume from the full dataset is associated with a high probability of yielding inaccurate results. The results indicate that the WSVE Set approach is an appropriate tool for selecting small, computationally efficient RVEs that accurately reflect the salient features of the much larger, full material dataset. RVEs identified by the presented selection scheme can be confidently used in pore-scale modeling studies to maximize the computational efficiency and improve the accuracy of model predictions regarding the structure-performance relationship.

## Acknowledgements

This work was partially supported by the U.S. Department of Education's GAANN program (Award #P200A100145) and the National Science Foundation (NSF, Grant #1066623). The authors acknowledge support for instrumentation from the NSF Grant #DMR-0722845. The authors would also like to thank Dr. Craig L. Johnson (Centralized

Research Facilities, Drexel University) and David M. Turner (Mechanics of Microstructures Group, Drexel University) for their guidance in FIB-SEM operation and WSVE Set selection, respectively.

## References


1. R. Borup, J. Meyers, B. Pivovar, Y. S. Kim, R. Mukundan, N. Garland, D. Myers, M. Wilson, F. Garzon, D. Wood, P. Zelenay, K. More, K. Stroh, T. Zawodzinski, J. Boncella, J. E. McGrath, M. Inaba, K. Miyatake, M. Hori, K. Ota, Z. Ogumi, S. Miyata, A. Nishikata, Z. Siroma, Y. Uchimoto, K. Yasuda, K. Kimijima, and N. Iwashita, *Chemical Reviews*, **107**, 3904 (2007).
2. K. Jiao and X. Li, *Progress in Energy and Combustion Science*, **37**, 221 (2011).
3. R. P. Ramasamy, E. C. Kumbur, M. M. Mench, W. Liu, D. Moore, and M. Murthy, *International Journal of Hydrogen Energy*, **33**, 3351 (2008).
4. U. Pasaogullari and C. Y. Wang, *Electrochimica Acta*, **49**, 4359 (2004).
5. T. Swamy, E. C. Kumbur, M. M. Mench, *J. Electrochem. Soc.*, **157**, B77 (2010).
6. H. Bajpai, M. Khandelwal, E. C. Kumbur, and M. M. Mench, **195**, 4196 (2010).
7. J. T. Gostick, M. A. Ioannidis, M. W. Fowler, and M. D. Pritzker, *J. Power Sources*, **173**, 277 (2007).
8. M. Rebai and M. Prat, *Journal of Power Sources*, **192**, 534 (2009).
9. R. Wu, X. Zhu, Q. Liao, H. Wang, Y. Ding, J. Li, and D. Ye, *International Journal of Hydrogen Energy*, **35**, 9134 (2010).
10. P. K. Sinha and C. Wang, *Chemical Engineering Science*, **63**, 1081 (2008).
11. K. Lee, J. Nam, and C. Kim, *Electrochimica Acta*, **54**, 1166 (2009).
12. J. Hinebaugh, Z. Fishman, A. Bazylak, *J. Electrochem. Soc.*, **157**, B1651 (2010).
13. J. Park and X. Li, *Journal of Power Sources*, **178**, 248 (2008).
14. T. Koido, T. Furusawa, and K. Moriyama, *J. Power Sources*, **175**, 127 (2008).
15. H. Ostadi, P. Rama, Y. Liu, R. Chen, X.X. Zhang, and K. Jiang, *Journal of Membrane Science*, **351**, 69 (2010).
16. K. Jiao and B. Zhou, *Journal of Power Sources*, **175**, 106 (2008).
17. J. W. Park, K. Jiao, and X. Li, *Applied Energy*, **87**, 2180 (2010).
18. E.C. Kumbur, K.V. Sharp, M.M. Mench, *J. Power Sources*, **168**, 356 (2007).
19. S. R. Niezgoda, D. M. Turner, D. T. Fullwood, and S. R. Kalidindi, *Acta Materialia*, **58**, 4432 (2010).
20. H. Iwai, N. Shikazono, T. Matsui, H. Teshima, M. Kishimoto, R. Kishida, D. Hayashi, K. Matsuzaki, D. Kanno, M. Saito, H. Muroyama, K. Eguchi, N. Kasagi, H. Yoshida, *Journal of Power Sources*, **195**, 955 (2010).
21. B. J. Inkson, M. Mulvihill, G. Mobus, Scripta Materialia, **45**, 753 (2001).
22. T. W. Ridler and S. Calvard, *IEEE Trans.*, **SMC-8**, 630 (1978).
23. H. Tang, S. Wang, M. Pan, and R. Yuan, *J. Power Sources*, **166**, 41 (2007).
24. S. R. Niezgoda, D. T. Fullwood, S. R. Kalidindi, *Acta Mater.*, **56**, 5285 (2008).
25. D. T. Fullwood, S. R. Niezgoda, B. L. Adams, S. R. Kalidindi, *Progress in Materials Science*, **55**, 477 (2010).
26. E. W. Dijkstra, *Numerische Mathematik*, **1**, 269 (1959).
27. A. Cecen, E. A. Wargo, A. C. Hanna, D. M. Turner, S. R. Kalidindi, and E. C. Kumbur, *Journal of Power Sources*, in review (2011).
28. J. G. Berryman, *Journal of Mathematical Physics*, **28** (1), 244 (1987).